A LOW-COST METHOD FOR MANUFACTURING WIND TUNNEL MODELS USING 3D PRINTING

*Filipe Jiro Shimizu Pereira[1], Joel Laguárdia Campos Reis[2], Samuel Leão Lopes[1], Gabriel Teixeira Reis[1], Filipe Arantes Afonso de Almeida[1]

[1]Center of Aeronautical Studies, Federal University of Minas Gerais, Minas Gerais, Brazil
[2]0000-0003-2847-573X, Center of Aeronautical Studies, Federal University of Minas Gerais, Minas Gerais, Brazil
*corresponding author: *filipe.jiro@gmail.com*

Keywords: 3D printing, wind tunnel model, low-cost manufacturing, structural validation, composites

Abstract: This paper presents the development of a low-cost methodology for manufacturing wind tunnel models using additive manufacturing techniques. The motivation of the study lies in the fact that traditional wind tunnel models require highly specialized labour and expensive machinery, making the process costly and time-consuming. Hence, the proposed method leverages 3D printing to fabricate models with complex geometries while integrating internal reinforcements to ensure structural integrity, as the use of 3D printers represents a wise and simplified alternative to the issues encountered in the traditional way of wind tunnel fabrication.

The development process involved constructing multiple test bodies with different printing configurations to determine the optimal balance between structural quality and surface finish, enabling model validation. Destructive testing was conducted to validate the mechanical properties of the models, demonstrating that strategic reinforcements, such as aluminium or steel tubes and composite materials, significantly enhance structural performance. The results indicate that 3D printing can serve as a viable alternative for producing validated wind tunnel models, reducing manufacturing costs and broadening accessibility to aerodynamic testing.

ID number: IIICAB-28

1 INTRODUCTION

The development and validation of aeronautical projects are strongly dependent on wind tunnel testing, which requires the use of physical models representative of real flight configurations. Traditionally, such models are produced from high-strength metallic or composite materials, a process that entails elevated costs and long production times. In this context, the integration of additive manufacturing technologies with alternative materials such as polylactic acid (PLA) presents a promising pathway to accelerate prototyping stages and reduce expenses during the early phases of development.

This study examines the feasibility of PLA as a material for the fabrication of aircraft models intended for wind tunnel applications, with particular emphasis on its structural performance. Owing to its low cost and ease of processing, PLA enables the rapid construction of complex geometries; however, its suitability in scenarios involving significant mechanical loads remains subject to further scrutiny. Beyond the fabrication and assembly of models, this work seeks to evaluate the structural limits of PLA under the stresses and loads typical of aerodynamic testing environments, thereby contributing to the assessment of its applicability in contexts where mechanical integrity is essential. By analysing potential failure modes, stiffness, and the inherent constraints of the printing process, the research aims to establish technical guidelines for the safe and efficient use of PLA in experimental aerodynamic investigations.

2 METHODOLOGY

The methodology adopted in this study initially involved the printing of a scaled-down aircraft model, which served as a reference for preliminary tests regarding surface finish and manufacturing feasibility. The dimensions and geometry of this model were taken from reference [1], which presents a generic small aircraft configuration widely used in experimental aerodynamic studies. Subsequently, Figures 1, 2, and 3 illustrate the sketch of the aircraft manufactured using PLA.

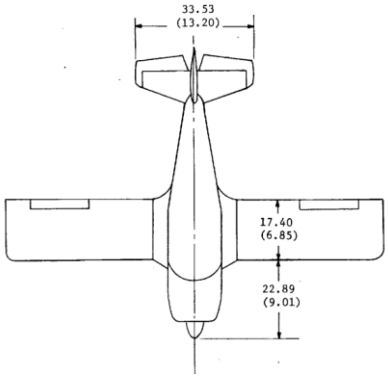

Figure 1. Top view of the sketch used, with measurements in centimetres. Available at [1, p. 11].

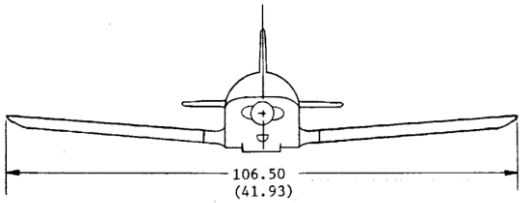

Figure 2. Frontal view of the sketch used, with measurements in centimetres. Available at [1, p. 11].

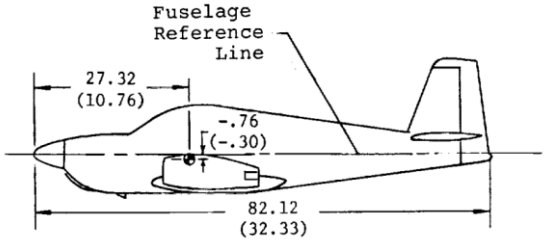

Figure 3. Side view of the sketch used, with measurements in centimetres. Available at [1, p. 11].

For the initial prototype, a scale factor of 0.75125 was applied to the reference dimensions illustrated in Figures 1, 2, and 3, resulting in a wingspan of 31.5 cm and an overall length of 25.5 cm (nose to tail). This preliminary model was employed to assess the quality of the 3D printing process and to verify the feasibility of obtaining a surface finish suitable for wind tunnel testing after sanding and painting. Following the satisfactory outcomes of this stage, Test Version 1 was manufactured—an enlarged configuration with double the linear dimensions of the initial model, while preserving the same geometric characteristics.

Subsequently, Test Version 2 was produced, consisting exclusively of the left wing and incorporating two vertical copper reinforcements positioned at approximately one-quarter of the chord length. This configuration was designed to investigate the influence of internal structural reinforcements on the mechanical performance of the model.

All prototypes were fabricated in PLA using an Ender 5 Plus 3D printer, configured with 30% triangular infill and four solid perimeters (walls). The geometric design was developed in Fusion 360, and the slicing process was performed with OrcaSlicer. Test Versions 1 and 2 underwent destructive testing to evaluate structural stiffness, identify failure modes, and examine the effects of reinforcements on overall integrity.

The material employed in this study was 1.75 mm white PLA from the brand 3DFila, manufactured using American raw material from the Ingeo line by NatureWorks [2]. Classified as a biopolymer due to its derivation from renewable sources such as corn and sugarcane, PLA is widely adopted in additive manufacturing owing to its dimensional stability, ease of extrusion, and ability to produce high-quality surface finishes. The specific formulation adopted by 3DFila is based on Ingeo 4043D [3], one of the most widely

used grades for 3D printing worldwide. Table 1 summarizes the key mechanical properties of this grade, as reported in [4].

Table 1. Mechanical properties of Ingeo 4043D grade. Available at [4].

Physical Properties	Igeo Resin	ATSM Method
Tensile Yield Strength, MPa	60	D882
Tensile Strength at Break, MPa	53	D882
Tensile Modulus, MPa	3.6	D882
Flexural Strength, MPa	83	D790
Flexural Modulus, MPa	3.8	D790

Among the most relevant mechanical properties for the purposes of this study are a modulus of elasticity of approximately 3.6 GPa, a tensile strength typically ranging between 53 and 60 MPa, and a flexural strength of about 83 MPa. These values indicate that PLA is suitable for small-scale structural testing, allowing the assessment of stiffness, fracture resistance, and failure mechanisms under controlled loading conditions. Although its impact and fatigue resistance are comparatively lower than those of composite materials, PLA provides sufficient stiffness to withstand significant loads in destructive testing of 3D-printed prototypes.

An additional advantage of this material lies in its strong interlayer adhesion, low thermal shrinkage, and high geometric fidelity during the printing process, which enable the fabrication of models with accurate dimensions and high-quality surface finishes. These characteristics are particularly relevant when integrating printed models into aerodynamic experiments that demand well-defined geometries and surface integrity.

In the slicing and preparation stage, priority was given to optimizing surface finish. To this end, printing orientations were selected to favour longer and more continuous deposition paths in areas directly exposed to airflow, particularly on the wing surfaces. This strategy minimized the surface roughness typically associated with fused filament fabrication, thereby facilitating sanding and painting operations and ensuring a cleaner and more uniform final appearance.

Taken together, the combination of low cost, ease of processing, adequate mechanical performance, and favourable post-processing characteristics supports the selection of PLA as the base material for the fabrication of the models employed in this study, reinforcing its applicability in the structural evaluation of 3D-printed aeronautical prototypes.

2.1 Initial Boundary Conditions

The boundary conditions for both the numerical simulation and the structural tests were initially established. The load that the structure should withstand was determined considering the most critical operating condition expected during wind tunnel testing, based on the limitations of the facility available at the Federal University of Minas Gerais (UFMG). Under the maximum operating parameters permitted by this tunnel—namely, a flow velocity of 100 m/s and an air density of 1.225 kg/m³—the aerodynamic load was estimated assuming a maximum angle of attack of 15°, as reported in the reference study from which the model geometry was obtained. This angle corresponds to a maximum lift coefficient (CLmax) of approximately 1.3.

Based on these conditions, and considering a wing area of 0.066 m² and a wingspan of 0.63 m, the total lift force was calculated to be approximately 524 N (equivalent to 53 kgf). When symmetrically distributed, this force corresponds to 26.7 kgf acting on each wing. For the simulations, the load was applied at a critical point along the semi-span, located 0.134 m from the wing root, corresponding to the region of maximum loading in an elliptical lift distribution. In both the numerical analyses and the experimental tests, the model was fixed at the base of the fuselage, reproducing the mounting conditions of the wind tunnel.

2.2 Structural Analysis using the Finite Element Method

After the definition of the ideal loads and boundary conditions, a finite element analysis was carried out using the Finite Element Modeling and Postprocessing (FEMAP) software, with the purpose of obtaining an initial prediction of the stresses acting on the structure. During the simulation process, several indications emerged that the numerical model would exhibit discrepancies when compared to the physical prototypes. These differences were attributed primarily to the absence of reliable mechanical property data for the material employed, the challenges in accurately representing the internal infill patterns generated by the printing process, and the variability of the mechanical response in regions of geometric transition, often influenced by thermal and structural effects inherent to the manufacturing process.

For the unreinforced configuration, solid elements were employed together with orthotropic material properties to represent PLA. To reduce computational complexity and to facilitate the application of boundary conditions, only a portion of the geometry was modelled. Under these conditions, structural failure was predicted to occur at the most critical location under an applied load of 14 kg. The reinforced configuration was analysed following the same methodology; however, a rectangular copper beam was incorporated to represent the reinforcement. This element was modelled with solid elements and isotropic material properties, with its geometry and material definition based on the resources available in the laboratory. The results indicated that the copper reinforcement carried the majority of the induced stresses. Figure 4 presents the finite element analyses for the unreinforced and reinforced configurations, respectively, in which the blue and green regions denote areas of higher stress concentration.

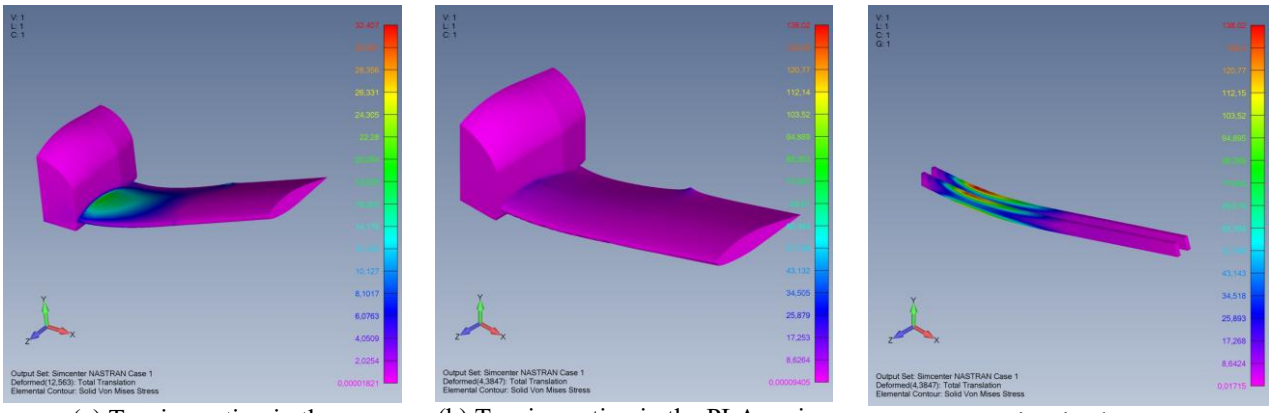

(a) Tension acting in the unreinforced model.

(b) Tension acting in the PLA region of the reinforced model.

(c) Tension in the copper reinforcement.

Figure 4. FEMAP analysis of the models with and without reinforcement.

2.3 Model Construction

Following the finite element analysis, three models were constructed, as it follows.

2.3.1. Prototype

The initial configuration, with a wingspan of 31.5 cm and a length of 25.5 cm, represented the complete aircraft and was intended to validate the surface finish attainable on a 3D-printed part at half the scale of the final model. The printer was configured with the same structural parameters employed for all subsequent configurations, and the surface finish settings were established. Furthermore, the finishing process was evaluated by applying a plastic filler to the model, followed by sanding, in order to achieve the desired surface quality.

Figure 5. The prototype model.

2.3.2. Test Version 1

The second configuration, designated as Test Version 1, with a wingspan of 63.0 cm and a length of 51.0 cm, was fabricated to evaluate the necessity of an internal reinforcing structure within the wing to withstand the applied stresses. Printing was performed in the final configuration for this model, which was also employed to validate the boundary conditions established for the destructive tests.

Figure 6. Test Version 1.

2.3.3. Test Version 2

The third configuration, designated as Test Version 2 and corresponding to the left wing of Test Version 1 with an internal copper structure, was intended to demonstrate that the incorporation of internal reinforcement within the wing enabled the construction of a 3D-printed prototype capable of withstanding the stresses encountered during wind tunnel testing. The internal structure consisted of two solid copper bars, each with a thickness of 3.2 mm, extending from the wing root to the tip and oriented vertically to connect the upper (extrados) and lower (intrados) surfaces of the airfoil. The first bar was positioned 32.6 mm from the leading edge at the wing tip, while the second was located 45.4 mm from the leading edge, thereby providing reinforcement in regions subjected to higher expected bending moments. This configuration was designed to increase local stiffness, redistribute internal loads, and delay or prevent structural failure under the applied aerodynamic forces.

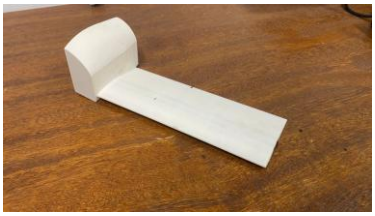

Figure 7. Test Version 2.

3 RESULTS AND DISCUSSION

Following the fabrication of the models and the execution of the planned destructive tests, the structural behaviour of the different PLA configurations was evaluated. The conducted tests enabled the identification of predominant failure modes and facilitated a comparative analysis of the effects of incorporating internal reinforcing structures within the wings.

The initial configuration, printed at half the scale of the final model, exhibited high geometric fidelity and good interlayer adhesion, which promoted a uniform surface finish, particularly on the wing and fuselage. The results obtained in this stage confirmed the feasibility of employing PLA for the production of models that satisfy the predefined geometric tolerances and surface quality required for wind tunnel testing.

The second configuration, representing the aircraft in its final geometry but without internal reinforcements, was subjected to an incremental vertical load applied at 40% of the left wing's span. Structural failure was observed at a load of 8 kg, significantly lower than the value predicted by the finite element analysis, and was concentrated in the wing root region. This result highlighted a critical point of stress concentration and revealed the structural limitations of PLA at the wing-fuselage interface. It had been anticipated that this region would experience the highest stress levels and exhibit greater material fragility, resulting from the variability of PLA's mechanical properties in areas with abrupt geometric transitions.

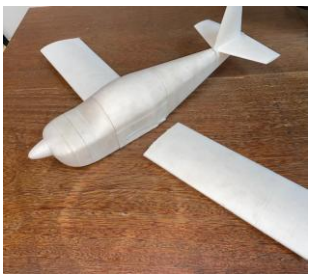

Figure 8. Failure of Test Version 1.

Subsequently, the third configuration, incorporating two rectangular copper beams embedded within the thickest region of the airfoil, was tested. The internal reinforcement was intended to redistribute stresses and enhance the structural stiffness of the wing. The reinforced model exhibited markedly improved performance, sustaining a load of 30 kg prior to failure. Unlike the previous configuration, however, structural failure occurred in the fuselage region, near the wing-fuselage junction, indicating a more fragile area within the model. The observed failure mode suggests that the internal reinforcements effectively increased the wing's load-bearing capacity, resulting in a shift of the critical point to previously unreinforced regions.

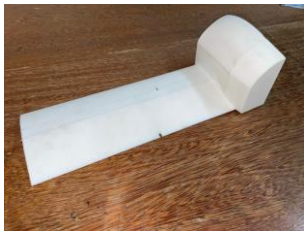

Figure 9. Failure of Test Version 2.

The structural performance of the configuration incorporating internal reinforcement provided critical insights into the mechanical behavior of PLA-printed components under concentrated loading. The inclusion of two rectangular copper beams, strategically positioned within the thickest region of the airfoil, was found to be effective in redistributing internal stresses throughout the wing structure. Consequently, a substantial increase in load-bearing capacity was observed, with the reinforced model sustaining 30 kg prior to failure—significantly exceeding the anticipated operational load in the wind tunnel scenario.

Figure 10. How the tests were conducted.

Notably, structural failure did not occur within the reinforced wing region but instead at the junction between the fuselage and the wing root. This shift in the failure location underscores the effectiveness of the reinforcement strategy while simultaneously revealing a critical limitation: by locally increasing the stiffness of the wing, the structure redirected stress to an adjacent, structurally weaker zone. Such behavior is consistent with classical failure propagation patterns in heterogeneous structures, in which local reinforcement alters the global stress distribution. Consequently, the wing no longer represented the critical region under load, and attention must be directed toward ensuring structural continuity and strength across the entire airframe, particularly at interface zones such as wing-fuselage connections.

Additionally, the results highlight other factors that influence the structural integrity of 3D-printed models beyond reinforcement alone. Parameters such as printing orientation, wall thickness, layer adhesion, and infill density play a decisive role in determining how loads are transmitted and absorbed throughout the geometry. Regions not initially anticipated to fail may become vulnerable due to the anisotropic mechanical

behaviour typical of additive manufacturing. Inter-layer weaknesses or geometric transitions—such as those occurring near fillets, junctions, or curvature changes—may act as initiators of premature failure, especially where sharp stiffness gradients exist between reinforced and unreinforced sections.

Furthermore, although the incorporation of internal reinforcements effectively increased the load-bearing capacity, it introduces additional considerations regarding printability, material compatibility, and accessibility of the internal geometry. Careful planning is required to embed reinforcements within the printed volume, particularly for models manufactured in multiple parts. Interfaces between printed modules, if inadequately designed, can become structural discontinuities, undermining the benefits of reinforcement and compromising the overall stiffness of the model. These findings indicate that an integrated design approach is essential, one that simultaneously accounts for material behavior, geometric design, and manufacturing constraints.

4 CONCLUSIONS

The study demonstrated that it is feasible to fabricate a 3D-printed model capable of withstanding the mechanical loads required for wind tunnel testing, while simultaneously achieving adequate surface quality for aerodynamic evaluation. The adoption of additive manufacturing significantly reduced both the cost and time associated with the fabrication process compared to traditional methods. Nevertheless, the results clearly indicate that internal structural reinforcements are essential to ensure mechanical integrity under operational loading conditions. The unreinforced configuration failed under the anticipated design load, whereas the reinforced version successfully sustained the applied forces, confirming the effectiveness of the embedded strengthening elements.

Moreover, the success of this approach depends not only on reinforcement strategies but also on the application of appropriate printing techniques and the use of high-quality, reliable filament. Parameters such as print orientation, layer adhesion, wall thickness, and infill density exerted a decisive influence on the mechanical behaviour of the final structure. Similarly, the use of a consistent and well-characterized PLA—such as Ingeo 4043D—proved fundamental in ensuring reproducible results and predictable structural performance. Collectively, these findings underscore that, although additive manufacturing represents a viable alternative for the rapid prototyping of aerodynamic models, its effectiveness is contingent upon an integrated approach that simultaneously considers design, material selection, and manufacturing process optimization.

It is proposed that future work further validates this manufacturing methodology, incorporating improved techniques for model finishing and reinforcement of additional geometric regions. Furthermore, it is recommended that wind tunnel tests be conducted to compare models produced using the methodology described herein with those manufactured through traditional techniques, thereby enabling a comprehensive assessment of performance and reliability.

4.1 Declaration of Competing Interest

The authors declare no conflict of interest.

5 REFERENCES

[1] Bihrle WB Jr, Barnhart B, Pantason P (1978) Static Aerodynamic Characteristics of a Typical Single-Engine Low-Wing General Aviation Design for an Angle-of-Attack Range of -8° to 90°. NASA Contractor Report 2971.

[2] 3DFila (n.d.) PLA filament. Available at: https://3dfila.com.br/categoria-produto/filamento-pla/ (Accessed 10 Jul 2025).

[3] NatureWorks LLC (n.d.) Home. Available at: https://www.natureworksllc.com/ (Accessed 10 Jul 2025).

[4] NatureWorks LLC (n.d.) Ingeo™ Biopolymer 4043D Technical Data Sheet: 3D Printing Monofilament – General Purpose Grade. Available at: https://www.natureworksllc.com/~/media/Files/NatureWorks/Technical-Documents/Technical-Data-Sheets/TechnicalDataSheet_4043D_3D-monofilament_pdf.pdf (Accessed 10 Jul 2025).